Available online at www.sciencedirect.com
SCIENCE DIRECT®
Journal of Computational Physics 210 (2005) 225–246
JOURNAL OF COMPUTATIONAL PHYSICS
www.elsevier.com/locate/jcp

A conservative level set method for two phase flow

Elin Olsson *, Gunilla Kreiss

Department of Numerical Analysis and Computer Science, Royal Institute of Technology, Lindstedsvagen 3, 100 44 Stockholm, Sweden

Received 26 August 2004; received in revised form 8 April 2005; accepted 13 April 2005
Available online 21 June 2005

Abstract

A conservative method of level set type for moving interfaces in divergence free velocity fields is presented. The interface is represented implicitly by the 0.5 level set of a function Φ being a smeared out Heaviside function, i.e., a function being zero on one side of the interface and one on the other. In a transition layer of finite, constant thickness Φ goes smoothly from zero to one. The interface is moved implicitly by the advection of Φ, which is split into two steps. First Φ is advected using a standard numerical method. Then an intermediate step is performed to make sure that the smooth profile of Φ and the thickness of the transition layer is preserved. Both these steps are performed using conservative second order approximations and thus conserving $\int\Phi$. In this way good conservation of the area bounded by the 0.5 contour of Φ is obtained.

Numerical tests shows up to second order accuracy and very good conservation of the area bounded by the interface.

The method was also coupled to a Navier–Stokes solver for incompressible two phase flow with surface tension. Results with and without topological changes are presented.

Keywords: Level set method; Free boundary; Two phase flow; Incompressible flow; Conservative method

1. Introduction

Problems involving moving boundaries and interfaces exist in a wide range of applications, such as multi-phase flow, crystal growth, image processing, front propagations, fluid–structure interactions, etc. Different ways to simulate these problems have been developed. Some of the more commonly used are front tracking methods and level set methods and for incompressible flows volume of fluid methods.

* Corresponding author. Tel.: +46 8 790 71 87.
E-mail addresses: elino@kth.se, elol2270@nada.kth.se (E. Olsson), gunillak@nada.kth.se (G. Kreiss).

0021-9991/$ - see front matter © 2005 Elsevier Inc. All rights reserved.
doi:10.1016/j.jcp.2005.04.007

In the simulation of incompressible two phase flow volume of fluid (VOF) methods have been used extensively. In these methods, the interface is given implicitly by a color function, defined to be the fraction of volume within each cell of one of the fluids. From the color function, a reconstruction of the interface is made and the interface is then propagated implicitly by updating the color function. VOF methods are conservative and can deal with topological changes of the interface. However, they are often rather inaccurate, high order of accuracy is hard to achieve because of the discontinuity of the color function. As far as we know, no advection scheme for the volume of fluid method has order higher than two. Also, properties of the interface such as normal and curvature are hard to calculate accurately. Still, the good conservation properties are attractive and quite sophisticated methods have been developed. For one of the early work on VOF, we refer to Noh and Woodward [1] and for a review of this type of methods to Scardovelli and Zaleski [2].

Another approach for free boundary problems is to track the boundary explicitly by markers distributed evenly on the interface, and then propagate the markers. In this way the interface can be represented sharply. This type of methods are often referred to as front tracking methods. Markers may however move close together or far apart, making redistribution of markers necessary. Special care has to be taken to topological changes. Also, if the markers move independently of each other, oscillations in the interface may occur. Another difficulty is the interaction of the interface with a fixed Eulerian grid, which is often needed. All these features makes front tracking methods hard to implement for a general case. A method to simulate multi-fluid flows using front tracking is described in [3].

Lately, level set methods have become popular and have been used in a large variety of applications such as compressible and incompressible two phase flow, image processing and flame propagation, just to mention a few. General descriptions of level set methods can be found in [4,5] and applications to two phase flow in [6,7]. In general, the interface is represented by the zero contour of a signed distance function, the level set function. The movement of the interface is governed by a differential equation for the level set function. The advection is in general done by (weighted) essentially non-oscillatory (WENO, ENO) methods. To keep the level set function a signed distance function, a reinitialization process is needed. Also this process is governed by a differential equation. Level set methods automatically deal with topological changes and it is in general easy to obtain high order of accuracy, just by picking an ENO or WENO scheme with the desired order of accuracy.

One of the drawbacks of level set methods is that they are not conservative. For incompressible two phase flow, loss or gain of mass might occur, which is physically incorrect. The poor mass conservation of level set methods in a finite element framework compared to front tracking methods was pointed out in [8]. Several attempts to improve mass conservation of level set methods have been done. In [9], a combination of the level set method and the VOF method was used in order to obtain the good mass conservation of the VOF method, but using a level set function to obtain better approximations of the curvature. A color function is needed and has to be advected, as in standard volume of fluid schemes. Since this function is discontinuous across the interface special care has to be taken when advecting this function. Due to this, it might be hard to obtain advection schemes of order higher than two without introducing oscillations. The simplicity of the original level set methods is also lost. The problem of mass conservation of level set methods was also addressed in [10]. The authors there propose a hybrid level set – marker particles method to improve accuracy, in particular in underresolved regions. However, in both these cases the original simplicity of level set methods is partly lost.

Our goal is to find an alternative level set function, together with an advection scheme, resulting in conservation of the area (volume in 3 dimensions) bounded by the interface. The velocity field is assumed to be divergence free. To achieve our goal, we use a smeared out Heaviside function as the level set function, i.e., a function being zero in one fluid and one in the other. Over the interface it varies smoothly from zero to one. The advection of the level set function is performed using a conservative scheme with an intermediate

step that keeps the shape and width of the profile across the interface constant. Furthermore, our level set function will be smooth, which makes our method easy to extend to higher order, as opposed to the discontinuous color function.

2. Choice of level set function

In standard level set methods, the level set function Φ is defined to be a signed distance function

$$|\Phi(\vec{x})| = d(\vec{x}) = \min_{x_I \in I}(|\vec{x} - \vec{x}_I|),$$

where I is the interface, $\Phi(\vec{x}) > 0$ on one side of the interface and $\Phi(\vec{x}) < 0$ on the other. The advection of Φ, including a reinitialization step to retain Φ as a distance function, is not done in a conservative way, not even for divergence free velocity fields. This implies that the area bounded by the zero level set is not conserved. This is one of the drawbacks of level set methods.

To represent density and viscosity discontinuities over the interface the Heaviside function:

$$H(\Phi) = 0, \quad \Phi < 0,$$
$$H(\Phi) = 1, \quad \Phi > 0$$

is needed. In computations, to achieve numerical robustness, a smeared out Heaviside is often used. For example

$$H_{\mathrm{sm}}(\Phi) = \begin{cases} 0, & \Phi < -\epsilon, \\ \frac{1}{2} + \frac{\Phi}{2\epsilon} + \frac{1}{2\pi}\sin\left(\frac{\pi\Phi}{\epsilon}\right), & -\epsilon \leqslant \Phi \leqslant \epsilon, \\ 1, & \Phi > \epsilon, \end{cases} \tag{1}$$

where ϵ corresponds to half the thickness of the interface.

If we could instead choose

$$\widetilde{\Phi}(\vec{x}) = H_{\mathrm{sm}}(\Phi(\vec{x})),$$

we would not have to calculate H_{sm} from Φ. More important, assume we have a conservative numerical method to advect $\widetilde{\Phi}(\vec{x})$ that preserves the smooth profile of $\widetilde{\Phi}(\vec{x})$. Since the method is conservative $\int\Phi$ will be conserved exactly. This implies that we can also expect good conservation of $A_{\widetilde{\Phi}=0.5}$, the area bounded by $\widetilde{\Phi} = 0.5$, since $A_{\widetilde{\Phi}=0.5} \approx \int \Phi$. If we would use the sharp Heaviside, we would preserve the area exactly. However, on a discrete grid, the position of the interface is better approximated by the level set of a smooth function. The interface thickness should therefore typically depend on the grid size, so that the smooth profile can be resolved by the grid.

We can also choose to either define a sharp interface at $\widetilde{\Phi}(\vec{x}) = 0.5$ or a diffuse interface for $0 < \widetilde{\Phi}(\vec{x}) < 1$. In the following, we will refer to our choice of level set function as the phase field function, denoted Φ.

Normals and curvatures can easily be obtained from our phase field function as:

$$\hat{n} = \frac{\nabla\Phi}{|\nabla\Phi|},$$
$$\kappa = -\nabla \cdot \left(\frac{\nabla\Phi}{|\nabla\Phi|}\right).$$

3. Advection of the phase field function

3.1. Advective step

We now turn to the problem of finding a method to advect Φ that is conservative and that does not change the profile of Φ at the interface.

Assume the interface is advected with a given velocity field $\vec{u}$. This corresponds to the following simple ordinary differential equation for every point $\vec{x}$ on the interface

$$\frac{\mathrm{d}\vec{x}}{\mathrm{d}t} = \vec{u}(\vec{x}). \tag{2}$$

As in standard level set methods we can instead solve

$$\Phi_t + \vec{u} \cdot \nabla \Phi = 0 \tag{3}$$

on the entire domain. This will move the 0.5 level set of Φ according to (2). For incompressible flow, $\vec{u}$ is always divergence free, i.e., $\nabla \cdot \vec{u} = 0$. Eq. (3) is then equivalent to the conservation law

$$\Phi_t + \nabla \cdot (\Phi \vec{u}) = 0.$$

When choosing a suitable numerical method to solve this one has to consider:

- The method should be conservative.
- No spurious oscillations should be introduced.
- The thickness of the interface and the profile of Φ should be kept constant.

Using a uniform grid, we define grid points $\vec{x}_{i,j} = (x_i, y_i) = (x_0 + i\Delta x, y_0 + j\Delta y)$ and a grid function $\Phi_{i,j} \approx \Phi(\vec{x}_{i,j})$. The velocity, $\vec{u} = (u, v)$ is assumed to be given on a staggered grid, i.e., u on grid points $\vec{x}_{i+\frac{1}{2},j}$ and v on $\vec{x}_{i,j+\frac{1}{2}}$. Conservative methods can be written on the form

$$\frac{\mathrm{d}\Phi_{i,j}}{\mathrm{d}t} = -\frac{1}{\Delta x}(F_{i+\frac{1}{2},j} - F_{i-\frac{1}{2},j}) - \frac{1}{\Delta y}(G_{i,j+\frac{1}{2}} - G_{i,j-\frac{1}{2}}), \tag{4}$$

where $F_{i+\frac{1}{2},j}$ and $G_{i,j+\frac{1}{2}}$ approximates the flux $(F, G) = \Phi\vec{u}$ on the staggered grid. Calculating fluxes using centered averaging,

$$F_{i+\frac{1}{2},j} = 0.5(\Phi_{i,j} + \Phi_{i+1,j})u_{i+\frac{1}{2},j}, \quad G_{i+\frac{1}{2},j} = 0.5(\Phi_{i,j} + \Phi_{i,j+1})v_{i,j+\frac{1}{2}} \tag{5}$$

will typically introduce oscillations close to the interface. This can be seen in Fig. 1(b), which shows results after only a few time steps.

A large amount of work on TVD (total variation diminishing) methods has been done, see [11]. These methods approximate conservation laws without introducing oscillations near discontinuities. Linear TVD methods will however smear discontinuities. A suitable method for the advection of our phase field function would thus be a non-linear TVD method that does not smear discontinuities.

A typical TVD method uses an upwind scheme together with a piecewise linear reconstruction of Φ. A limiter has to be chosen to determine how the linear reconstruction is made. In time a conservative explicit second order Runge–Kutta discretization can be used. A more detailed description of this method is given in Appendix A. Results using different limiters, i.e., different Lim(x,y) in (A.1), are shown in Fig. 1(c)–(f). Here, a rotating velocity field (u,v) = (y,$-x$) was used. The figures show the result after one full revolution so that the initial state should be recovered exactly. We used the minmod, van Albada, van Leer and the Superbee limiter. Among TVD schemes, the ones using the Superbee limiter are well known to be the least

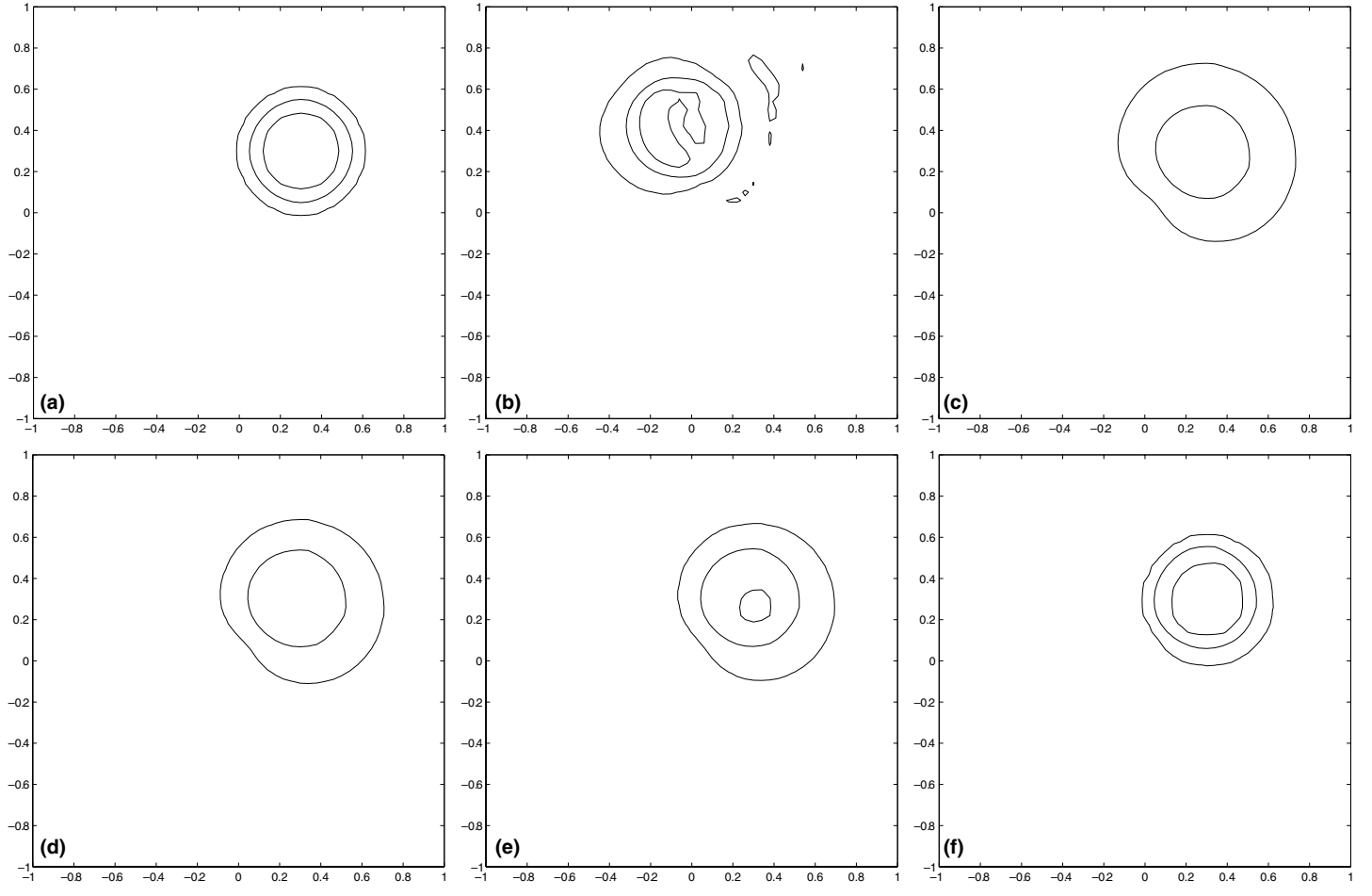

Fig. 1. 0.05, 0.5 and 0.95 Contours of Φ initially and after one revolution using different numerical methods. (c)–(f) are second order TVD methods, (b) is second order but not TVD. (a) Initial state; (b) centered differences; (c) upwind with Minmod; (d) upwind with Van Albada; (e) upwind with Van Leer; (f) upwind with Superbee.

diffusive, i.e., which will produce the least smearing. It is also clear from Fig. 1(c)–(f) that this limiter preserves the thickness of the interface better than the other limiters.

3.2. Intermediate step

Not even with the Superbee limiter (Fig. 1(f)), the profile and thickness of the interface remains constant. Also, the shape of the profile seems to depend on the normal of the interface relative the direction of motion. To solve this problem, we add an intermediate step after each time step that will make sure that the interface keeps its thickness and shape. As originally proposed by Harten [12] it is possible to add artificial compression in order to maintain the resolution of contact discontinuities. This can be viewed as an intermediate step where one is solving the conservation law

$$\Phi_\tau + \nabla \cdot \vec{f}(\Phi) = 0, \tag{6}$$

where $\vec{f}$ corresponds to the compressive flux. In our case, we want the artificial compression flux to act in regions where $0 < \Phi < 1$ and in the normal direction of the interface. To achieve this, we choose $\vec{f} = \Phi(1-\Phi)\hat{n}$, where $\hat{n}$ is the normal of the interface. We denote the time variable by τ to stress that this is an artificial time, not equivalent to the actual time t. We note that (6) is a hyperbolic differential equation. As τ increases, stationary shocks will develop at the interfaces.

To avoid discontinuities at the interface, we add a small amount of viscosity, i.e., we modify the conservation law by

$$\Phi_\tau + \nabla \cdot \vec{f}(\Phi) = \varepsilon \Delta \Phi \tag{7}$$

or in conservative form

$$\Phi_\tau + \nabla \cdot \tilde{f}(\Phi) = 0 \tag{8}$$

with

$$\tilde{f}(\Phi) = \vec{f}(\Phi) - \varepsilon \nabla \Phi.$$

By solving (8) to steady-state the interface thickness will remain constant and proportional to ε.

This can be approximated in space by

$$\frac{\mathrm{d}\Phi_{i,j}}{\mathrm{d}\tau} = -\frac{1}{\Delta x}(F_{i+1/2,j} - F_{i-1/2,j}) - \frac{1}{\Delta y}(G_{i,j+1/2} - G_{i,j-1/2}), \tag{9}$$

where F and G is the numerical flux at cell faces. We choose:

$$F_{i+1/2,j} = \frac{f(\Phi_{i,j}) + f(\Phi_{i+1,j})}{2} - \varepsilon \frac{\Phi_{i+1,j} - \Phi_{i,j}}{\Delta x},$$
$$G_{i,j+1/2} = \frac{g(\Phi_{i,j}) + g(\Phi_{i,j+1})}{2} - \varepsilon \frac{\Phi_{i,j+1} - \Phi_{i,j}}{\Delta y}$$

with f and g being the x and y components of $\vec{f}$. The interface normal $\hat{n} = \nabla\Phi/|\nabla\Phi|$ is approximated using centered differences:

$$(\nabla\Phi)_{i,j} = \frac{\Phi_{i+1,j} - \Phi_{i-1,j}}{2\Delta x}\hat{x} + \frac{\Phi_{i,j+1} - \Phi_{i,j-1}}{2\Delta y}\hat{y},$$
$$\hat{n}_{i,j} = \frac{(\nabla\Phi)_{i,j}}{|(\nabla\Phi)_{i,j}|}.$$

$\hat{n}_{i,j}$ is only calculated once in each intermediate step. That is, after each advection step, $\hat{n}_{i,j}$ is calculated and is then kept fixed until steady-state of (8) has been reached. In time we use the same Runge–Kutta approximation as for the advection of Φ. The method obtained is second order accurate in space and time.

Since we use explicit time stepping we get stability restrictions on $\Delta\tau$ due to the viscous term, typically

$$\Delta\tau \leqslant C\frac{(\Delta x)^2}{\varepsilon}.$$

Experimentally, we found that stability was obtained by choosing $C = 1/4$. We choose ε, which determines the interface thickness, to depend on the grid size in the following way:

$$\varepsilon = \frac{(\Delta x)^{1-d}}{2}.$$

If $d = 0$, ε and thus the width of the interface, will be proportional to Δx. In this case, the resolution of the smooth interface profile will not increase under grid refinement. As will be seen later we do, however, obtain second order accuracy even for $d = 0$ in a test calculation of a rotating circle. For a more complicated flow field, as the vortex test in Section 5.2, we had to choose $d > 0$ to obtain convergence. However, a small value, $d = 0.1$, was enough. In all our calculations we have used

$$\Delta\tau = \frac{(\Delta x)^{1+d}}{2}.$$

As a criteria for steady-state we used

$$\int |\Phi^{m+1} - \Phi^m| < \mathrm{TOL} \cdot \Delta\tau$$

for some specified tolerance TOL. Numerical tests have shown that in practice only a few time steps have to be performed in order to reach steady-state.

Results after one revolution using different methods for the advection together with the artificial compression step are given in Fig. 2. It is clear that we get reasonable solutions for all the advection methods, even the one using centered differences. The thickness of the interface is constant for each case.

3.3. Boundary and initial conditions on Φ

Appropriate boundary and initial conditions must also be assigned to Φ. In our calculations, we have either used $\Phi = 0$ on the boundaries or assumed the boundaries to be walls with a contact angle of $\theta = \pi$. In the case of walls, on the boundaries

$$\hat{n} \cdot \hat{n}_{\mathrm{wall}} = 0$$

should hold. Here $\hat{n}$ is the normal of the interface and $\hat{n}_{\mathrm{wall}}$ is the normal of the wall. This can be transformed to a homogeneous Neumann condition for Φ

$$\hat{n}_{\mathrm{wall}} \cdot \nabla\Phi = 0.$$

At $t = 0$, Φ has to be initiated. One way to do this is to set Φ to one on one side of the interface and zero on the other. Then (7) is solved numerically until a steady-state has been reached. The resulting function is used as initial data for Φ. However, in certain cases the steady-state of (7) can be found analytically. For steady-state, $\nabla \cdot \vec{f}(\Phi) = \varepsilon\Delta\Phi$ should hold and the 0.5 contour of Φ should lie along the desired interface. If

$$\Phi = \left(1 + \mathrm{e}^{(|\vec{x}-\vec{x}_c|-r)/\varepsilon}\right)^{-1},$$

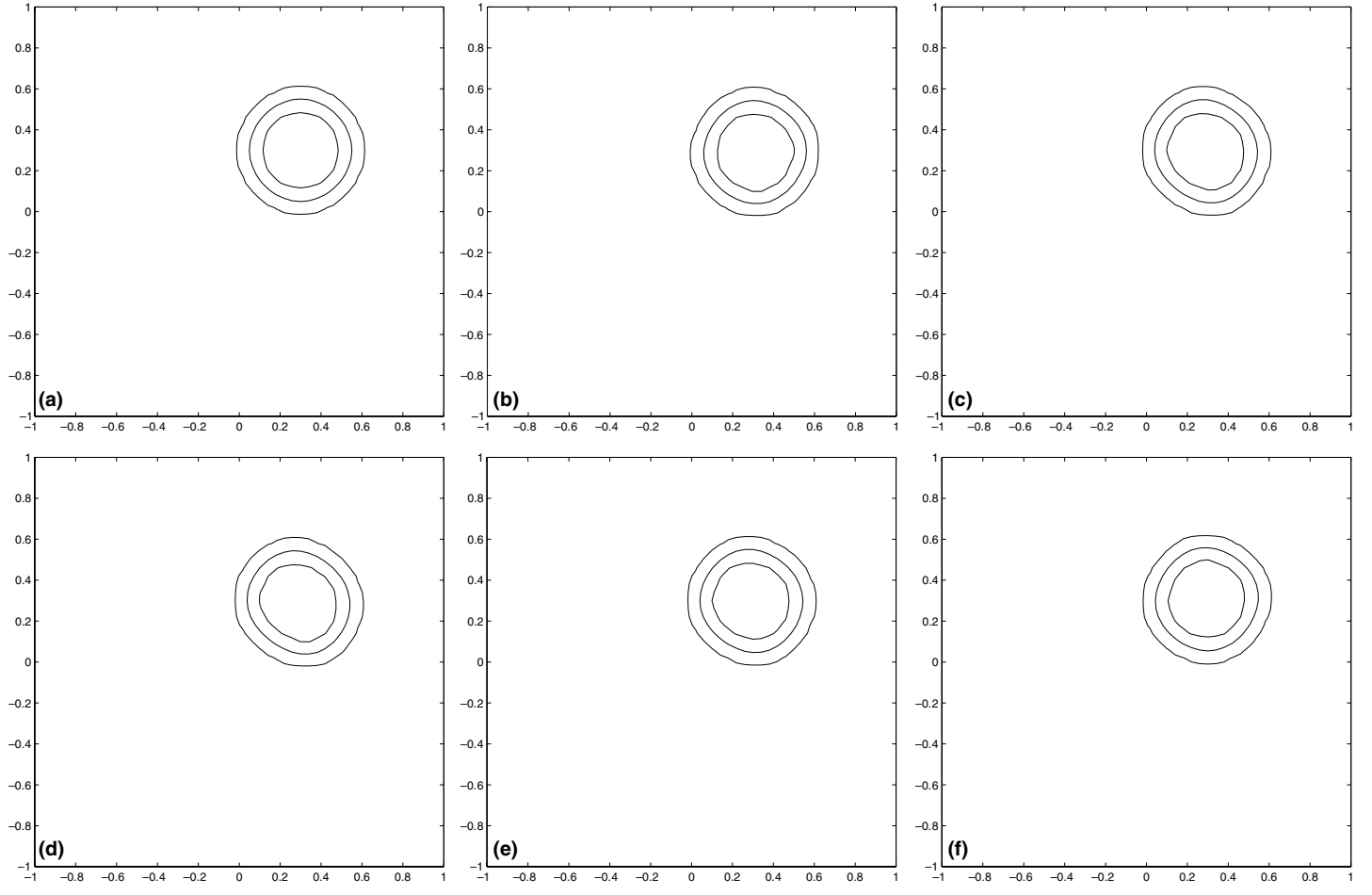

Fig. 2. Contours of Φ initially and after one revolution, $t = 2\pi$, using different methods together with the artificial compression step. (a) Initial state; (b) centered differences; (c) Van Albada; (d) upwind with Minmod; (e) upwind with Van Leer; (f) upwind with Superbee.

$\nabla \cdot \vec{f}(\Phi) = \varepsilon \Delta \Phi$ is fulfilled for $x \neq x_c$ and the 0.5 contour of Φ corresponds to a circle centered in $\vec{x_c}$ with radius r. Correspondingly for a horizontal interface at $y = y_{int}$ we can set

$$\Phi = \left(1 + e^{(y-y_{int})/\varepsilon}\right)^{-1}$$

to both fulfill steady-state and obtain the 0.5 contour at $y = y_{int}$.

4. Incompressible two phase flow

The next step is to couple our advection method for the phase field function with a two phase incompressible flow solver. We use a diffuse interface model, where surface tension is transformed to a volume force spread over a few layers of cells. The discontinuity in density and viscosity across the interface is also smoothed out.

Surface tension per interfacial area at a point $\vec{x}_I$ on the interface is given by

$$\vec{F}_{sa}(\vec{x}_I) = \sigma \kappa(\vec{x}_I)\hat{n}(\vec{x}_I).$$

As in [13] choosing a volume force at any point $\vec{x}$ as

$$\vec{F}_{sv}(\vec{x}) = \sigma\left(-\nabla \cdot \frac{\nabla \Phi}{|\nabla \Phi|}\right)\nabla \Phi$$

will result in the same total force as $\vec{F}_{sa}(\vec{x}_I)$, but spread over the finite interface width. Here, it becomes important that the thickness of the transition layer is kept constant. $\vec{F}_{sv}$ is equal to $\vec{F}_{sa}(\vec{x}_I)$ only in the limit when the thickness of the interface goes to zero. If the interface becomes wide $\vec{F}_{sv}$ will not be a good approximation of $\vec{F}_{sa}(\vec{x}_I)$. Therefore, the interface thickness should not become too wide. A too sharp transition, on the other hand, will yield difficulties in numerically computing $\vec{F}_{sv}$ accurately, since up to second order derivatives of Φ are needed.

The non-dimensionalized incompressible Navier–Stokes equations with surface tension and gravity are:

$$\nabla \cdot \vec{u} = 0, \tag{10}$$

$$\vec{u}_t + (\vec{u} \cdot \nabla)\vec{u} = -\frac{\nabla p}{\rho} + \frac{1}{\rho Re}\nabla \cdot \left(\mu\left(\nabla \vec{u} + (\nabla \vec{u})^T\right)\right) + \frac{1}{Fr^2}\vec{e}_g + \frac{1}{\rho We}\widetilde{F}_{sv}, \tag{11}$$

$$\Phi_t + \vec{u} \cdot \nabla \Phi = 0, \tag{12}$$

where $Re = \frac{\rho_{ref} u_{ref} l_{ref}}{\mu_{ref}}$ is the Reynolds number, $Fr = \frac{u_{ref}}{\sqrt{l_{ref} g}}$ the Froude number, $We = \frac{\rho_{ref} u_{ref}^2 l_{ref}}{\sigma}$ the Weber number and $\widetilde{F}_{sv} = \vec{F}_{sv}/\sigma$. $\vec{e}_g$ is the unit vector in the direction of gravitation, and ρ and μ the non-dimensionalized density and viscosity, respectively. The density and viscosity varies smoothly over the interface by letting:

$$\begin{aligned} \rho &= \rho_1 + (\rho_2 - \rho_1) \cdot \Phi, \\ \mu &= \mu_1 + (\mu_2 - \mu_1) \cdot \Phi \end{aligned} \tag{13}$$

with ρ_1, ρ_2 and μ_1, μ_2 being the dimensionless densities and viscosities of the two fluids, respectively.

We use a staggered grid for the discretization, i.e., Φ and p are given at grid points $\vec{x}_{i,j}$, whereas u is given on $\vec{x}_{i+1/2,j}$ and v on $\vec{x}_{i,j+1/2}$. Eqs. (10) and (11) are solved numerically using extensions of the Marker and Cell method [14] (see Appendix B for a thorough description) together with our conservative shape preserving advection scheme for the solution of (12). The pressure is updated implicitly by solving a Poisson equation with variable coefficients. This linear system is solved by a direct banded solver. The velocity is then

updated explicitly and finally Φ is advected with the calculated velocity. The method is second order accurate in space and first order in time.

Note that since we use conservative schemes for updating $\Phi_{i,j}$, $\int \Phi_{i,j} = \sum \Phi_{i,j}\Delta x\Delta y$ is conserved exactly. Since we define the density by (13), also $\int \rho_{i,j} = \sum \rho_{i,j}\Delta x\Delta y$ will be conserved. Mass is thus conserved exactly by our method.

5. Results

We tested our method on four different cases. First, two tests using our advection scheme for given divergence free velocity fields were investigated. Convergence studies were performed, including estimates of order of accuracy. Then, the advection was coupled to the Navier–Stokes solver described in Section 4 for the case of a rising air bubble in water. Finally, a test case involving topological changes of the interface was considered through a water droplet falling through air and then hitting a water surface.

In the two last simulations, the velocity component normal to the walls were set to zero on the boundary. For the tangential component homogeneous Neumann conditions were used. Homogeneous Neumann conditions were also used for Φ on all boundaries, i.e., a contact angle of π degrees. From these boundary conditions and the Navier–Stokes equations, Neumann conditions on the pressure follows, $\partial p/\partial x = 0$ on the vertical boundaries and $\partial p/\partial y = \rho/Fr^2$ on the horizontal ones.

5.1. Rotating circle

To test our advection scheme a circle was rotated in the constant velocity field $(u,v) = (y,-x)$. Solutions on different grids after one revolution, i.e., at $t = 2\pi$, were compared. The viscosity parameter in (7) was set to $\varepsilon = \Delta x/2$, so that the thickness of the transition layer gets smaller and smaller as the mesh becomes finer. Contour lines corresponding to $\Phi = 0.05$, 0.5 and 0.95 of the solutions at $t = 2\pi$ on four different grids, $\Delta x = 0.08$, 0.04, 0.02 and 0.01, with $\Delta t = \Delta\tau = \Delta x/2$ are shown in Fig. 3(a). Four artificial compression steps were performed after each time step. On the boundary we used $\Phi = 0$.

The conservation of the area within the 0.5 contour is shown in Fig. 3(b). Even though there is a small variation of the area, there is no drift, i.e., the maximum deviation from the initial area does not increase

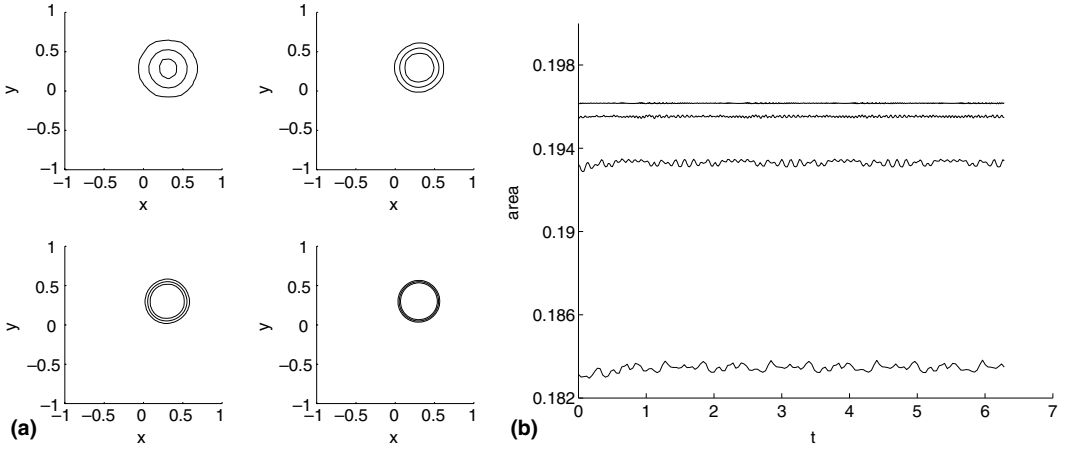

Fig. 3. Results on the different grids, upwind scheme with Superbee: (a) contour lines corresponding to $\Phi = 0.05$, $\Phi = 0.5$ and $\Phi = 0.95$ at $t = 2\pi$; (b) area conservation.

with time. On the coarsest grid we get a maximum deviation less than 0.5% and on the finest only 0.035%. The difference in initial area for the different grids is due to the discretization error of the initial Φ. Clearly from the result this error is of order $(\Delta x)^2$.

From the result, we estimated the order of accuracy with respect to the position of the circle and with respect to the error measured by

$$\int |H(\Phi_{\text{numerical}}) - H(\Phi_{\text{exact}})|/L \tag{14}$$

as was done in [7], where:

$$H(\Phi) = 0, \quad \Phi < 0.5, \tag{15}$$

$$H(\Phi) = 1, \quad \Phi > 0.5 \tag{16}$$

and L the perimeter size. In this way, we can measure the error of the sharp interface defined by $\Phi = 0.5$. The position of the bubble was defined by the center of mass:

$$X_{\text{center}} = \frac{\sum_{i,j} \Phi_{i,j} \cdot x_i}{\sum_{i,j} \Phi_{i,j}}, \quad Y_{\text{center}} = \frac{\sum_{i,j} \Phi_{i,j} \cdot y_j}{\sum_{i,j} \Phi_{i,j}}.$$

Calculated orders of accuracy are shown in the following table:

Δx	Order ($H(\Phi)$)	Order (y-pos)	Order (x-pos)
0.04	1.4	2.1	1.2
0.02	1.2	2.9	1.5
0.01	1.2	2.4	1.5

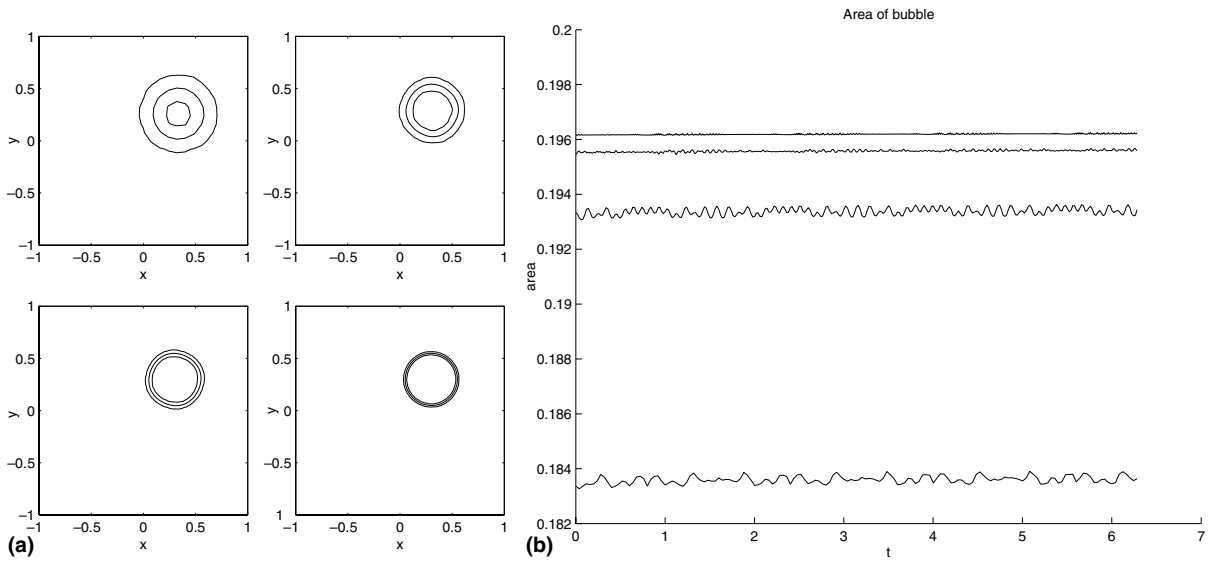

Fig. 4. Results on the different grids, central scheme: (a) contour lines corresponding to $\Phi = 0.05$, $\Phi = 0.5$ and $\Phi = 0.95$ at $t = 2\pi$; (b) area conservation.

In the previous calculations, we used the upwind scheme together with the piecewise linear reconstruction defined by the Superbee limiter. Exactly the same calculations were also done using the central scheme, i.e., (4) with (5). The obtained results are shown in Fig. 4(a) and (b).

The result is very similar to the result obtained with the Superbee scheme. Contours corresponding to the 0.5 level set of Φ are shown for each method in Fig. 5(a) and (b).

The following orders of accuracy were obtained:

Δx	Order ($H(\Phi)$)	Order (y-pos)	Order (x-pos)
0.04	2.0	2.2	2.0
0.02	1.8	2.1	1.9
0.01	2.0	2.0	1.9

We thus obtain higher order of accuracy for the central scheme, even though on the coarsest grid, the upwind scheme performs better.

5.2. Vortex test

To test our advection scheme on a more complicated flow, we used the following velocity field on the unit square:

$$u = \sin^2(\pi x)\sin(2\pi y),$$
$$v = -\sin^2(\pi y)\sin(2\pi x).$$

A circle with radius 0.15 centered at (0.5,0.75) was used as initial condition. At $t = T$ the flow field was reversed, so that the exact solution at $t = 2T$ should coincide with the initial condition. To obtain convergence, we had to choose $\varepsilon = (\Delta x)^{0.9}/2$. Computations on four grids (32^2, 64^2, 128^2, 256^2) were performed for

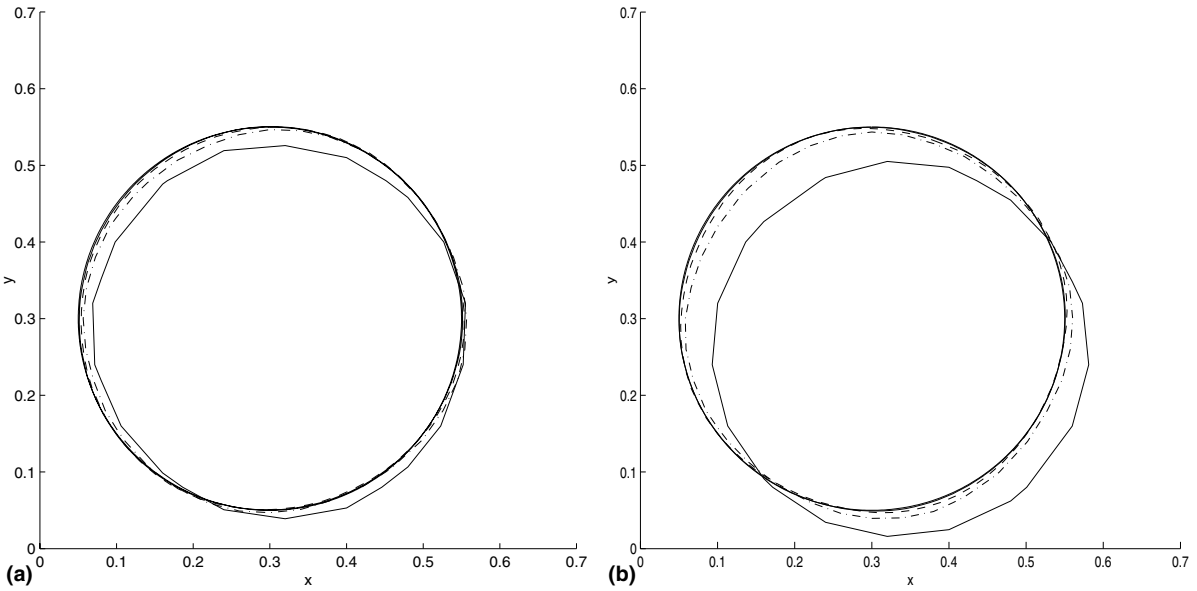

Fig. 5. 0.5 Contours of Φ, using different grids and different numerical methods: (a) upwind with Superbee; (b) central scheme.

$T = 1$ and $T = 0.5$. The solution for $T = 1$ at $t = 0$, $t = 0.5$, $t = 1$ and $t = 2$ are shown in Fig. 6. The conservation of the area bounded by the 0.5 contour, $T = 1$, is given in Fig. 7(a) and the 0.5 contours of Φ at $t = 2$ in Fig. 7(b). The corresponding results for $T = 0.5$ are shown in Fig. 8(a) and (b).

The results can be compared with results using standard level set method with reinitialization, see Figs. 9(a) and (b) and 10(a) and (b). Second order ENO schemes were used for both advection and reinitialization, cf. [6].

In Fig. 6, we note a pinch off as the thickness of the stretched circle gets close to the thickness of the interface. This is a numerical effect that can only be avoided if the thickness of the interface is smaller than the distance between two interfaces. We also note from Fig. 7(a) that this pinch off results in a small temporary mass loss. This mass loss is however small compared to the standard level set method, and the mass is recovered at $t = 2T$. For $T = 0.5$, the interface remains well resolved and the mass conservation is very good (Fig. 8(a)). Our method is clearly better with respect to mass conservation compared to the standard method. (Note the difference in scaling in Figs. 7(a), 9(a), 8(a) and 10(a).) This holds independently of whether the interface is well resolved or not.

As for the rotating bubble in previous section, we estimate the order of accuracy at $t = 2T$ with respect to the error defined by (14):

Δx	Error ($T = 1$)	Order ($T = 1$)	Error ($T = 0.5$)	Order ($T = 0.5$)
1/36	0.049		0.029	
1/62	0.025	0.97	0.0050	2.6
1/128	0.0023	3.5	0.0012	2.1
1/256	7.2×10^{-4}	1.7	4.7×10^{-4}	1.3

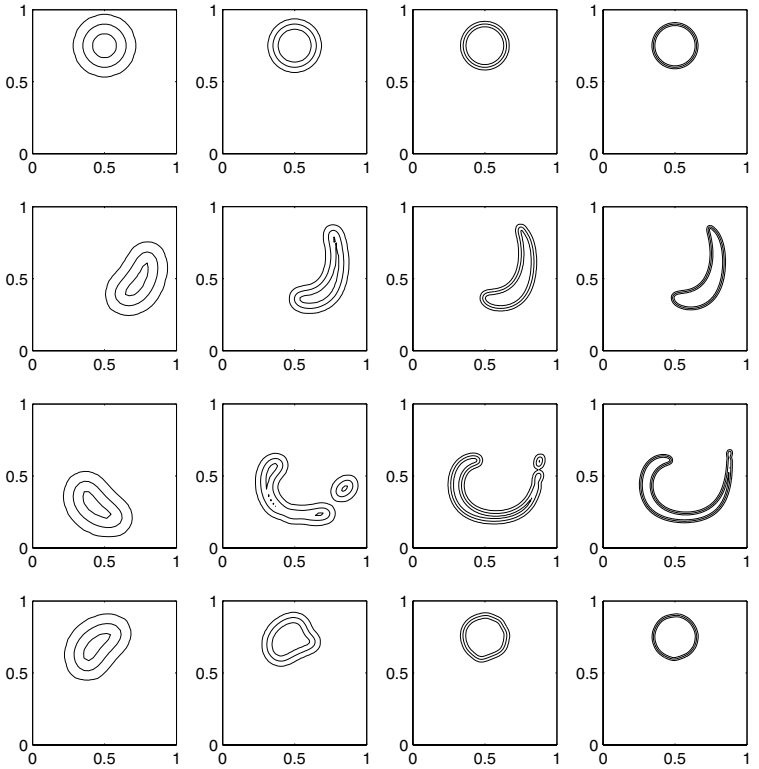

Fig. 6. Vortex test on four different grids at $t = 0$, $t = 0.5$, $t = 1$, $t = 2$. $T = 1$.

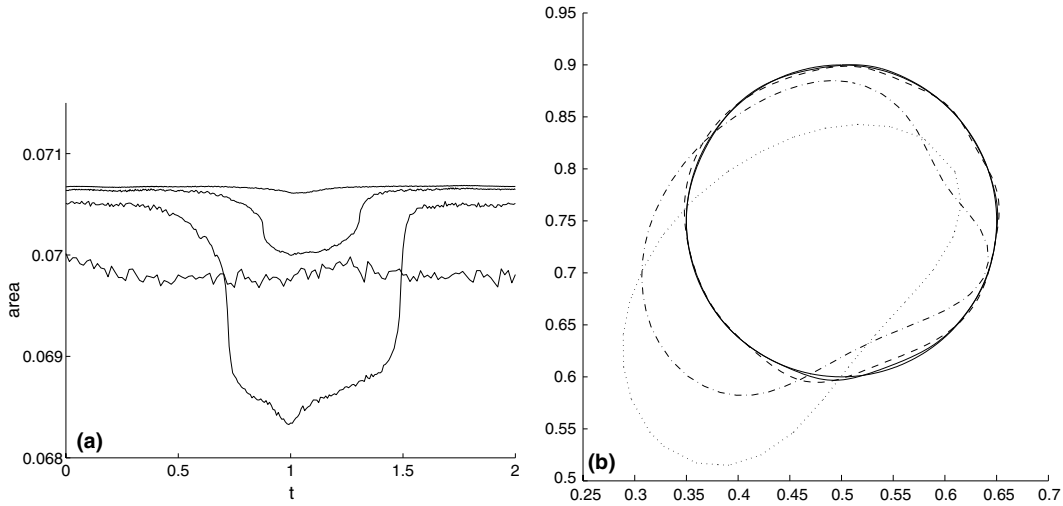

Fig. 7. Vortex test on four different grids, $T = 1$, using our method: (a) area conservation; (b) $t = 2$, 0.5 contour of Φ.

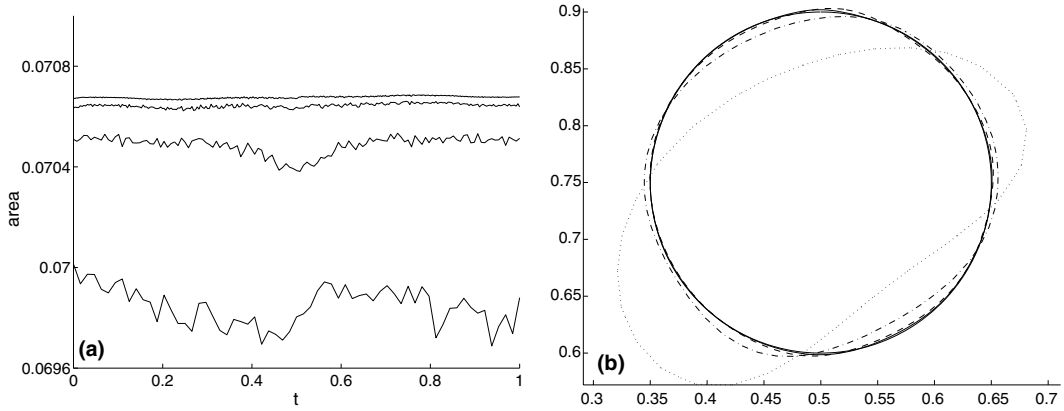

Fig. 8. Vortex test on four different grids, $T = 0.5$, using our method: (a) area conservation; (b) $t = 1$, 0.5 contour of Φ.

Finally, we performed a non-reversed simulation on the finest grid until $t = 4$. The solution at $t = 1$, $t = 2$, $t = 3$ and $t = 4$ is shown in Fig. 11. Clearly, the grid is not fine enough to resolve the interface.

5.3. Rising bubble

An air bubble in water initially at rest was studied. The reference density and viscosity was set to the density and viscosity of water: $\rho_{\text{ref}} = 1.0 \times 10^3$ kg/m^3, $\mu_{\text{ref}} = 1.0 \times 10^{-3}$ N s/m^2 so that $\rho_1 = 1$, $\rho_2 = 0.0013$, $\mu_1 = 1$, and $\mu_2 = 0.016$. Letting $\sigma = 7.3 \times 10^{-2}$ N/m, $l_{\text{ref}} = 5.0 \times 10^{-3}$ m and $u_{\text{ref}} = 0.1$ m/s, we obtain $Re = 500$, $Fr = 0.45$ and $We = 0.68$. Again, the interface thickness was determined by $\varepsilon = (\Delta x)^{0.9}/2$. We chose the time step by stability with respect to viscous and convective terms

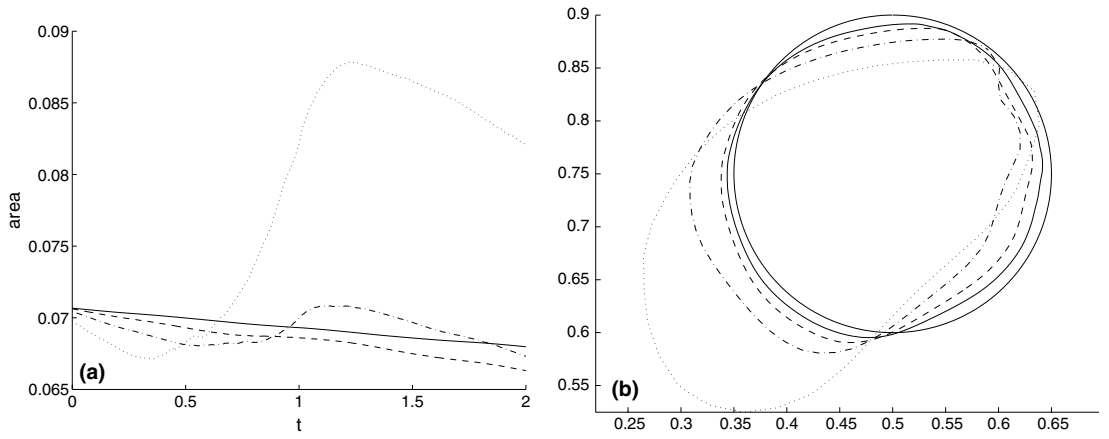

Fig. 9. Vortex test on four different grids, $T = 1$, using standard level set methods: (a) area conservation; (b) $t = 2$, 0 contour of Φ.

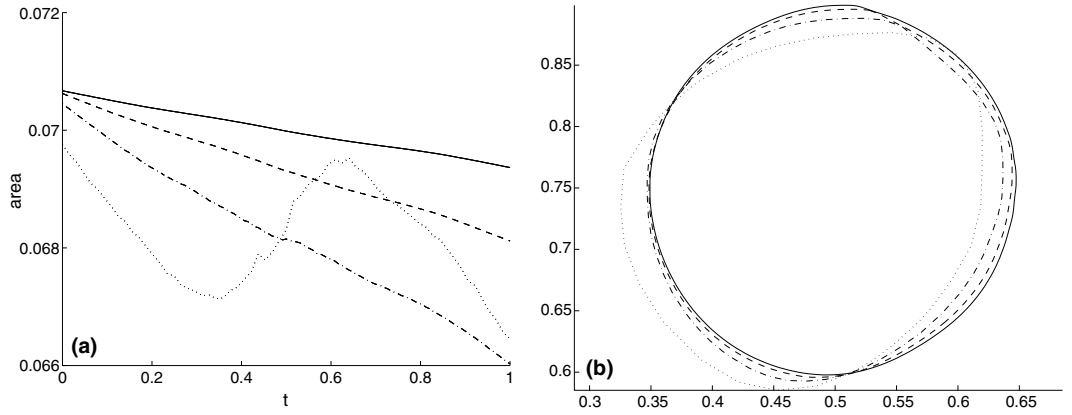

Fig. 10. Vortex test on four different grids, $T = 0.5$, using standard level set methods: (a) area conservation; (b) $t = 2$, 0 contour of Φ.

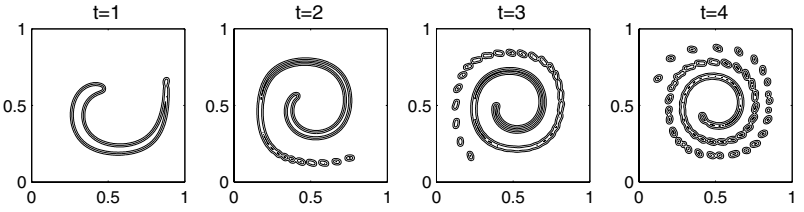

Fig. 11. Long time simulations.

$$\Delta t = 1 \Big/ \left(\frac{\max(|u|)}{\Delta x} + \frac{\max(|v|)}{\Delta y} + \frac{4}{\min(\rho \cdot Re/\mu)} \left(\frac{1}{(\Delta x)^2} + \frac{1}{(\Delta y)^2} \right) \right). \tag{17}$$

Results at $t = 0.5$ on the different grids, $\Delta x = 2/25$, $\Delta x = 2/50$, $\Delta x = 2/100$ and $\Delta x = 2/200$ are shown in Fig. 12. The time evolution of the area bounded by the 0.5 contour of Φ is shown in Fig. 13(a). The conservation is obviously very good. Even on the coarsest grid the area fluctuation is only about 0.1%. As in the other

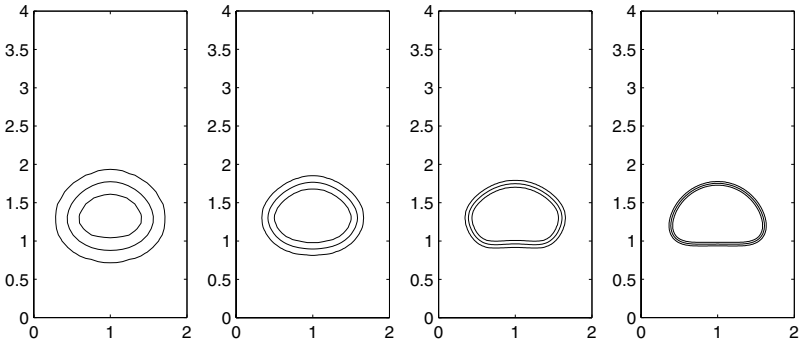

Fig. 12. Results at $t = 0.5$ of rising air bubble on four different grids.

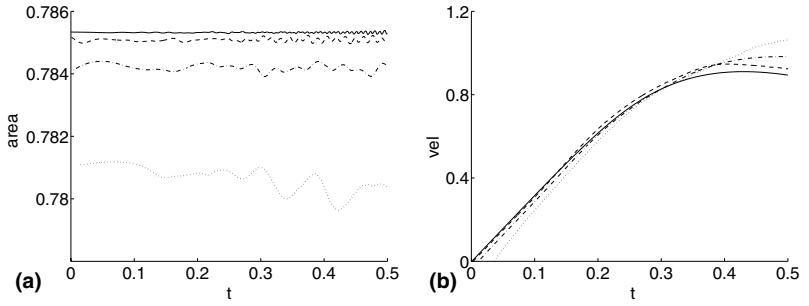

Fig. 13. Velocity of center of mass of bubble and area of region bounded by $\Phi = 0.5$: (a) area conservation; (b) velocities.

tests, the difference in initial area is due to the discretization error of the initial Φ. The velocity of center of mass is shown in Fig. 13(b) and the 0.5 contours of Φ in Fig. 14. The solid line corresponds to $\Delta x = 2/200$, the dashed to $\Delta x = 2/100$, the dashed-dotted to $\Delta x = 2/50$ and the dotted line to $\Delta x = 2/25$. We observe convergence of both the contours and the velocity, although the rate of convergence is rather slow. A possible reason for this can be the smearing of surface tension, viscosity and density.

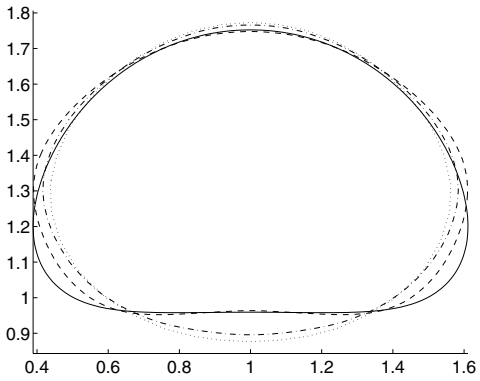

Fig. 14. Results at $t = 0.5$ of rising air bubble on four different grids.

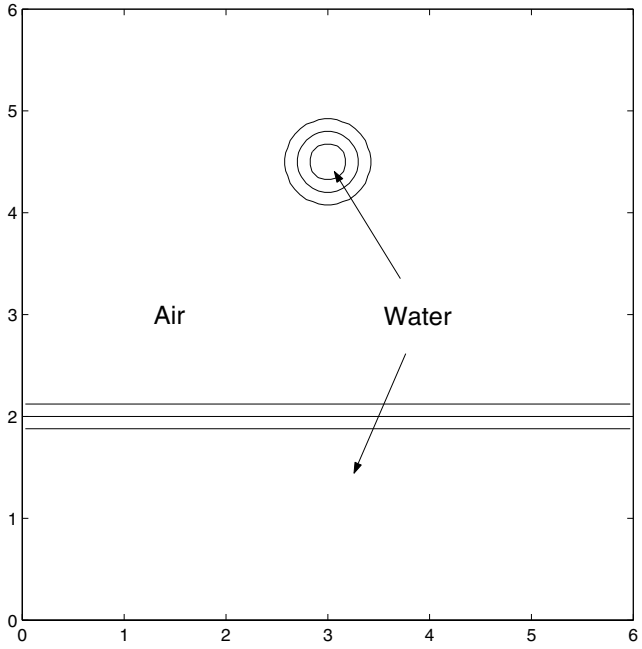

Fig. 15. Initial state of falling droplet.

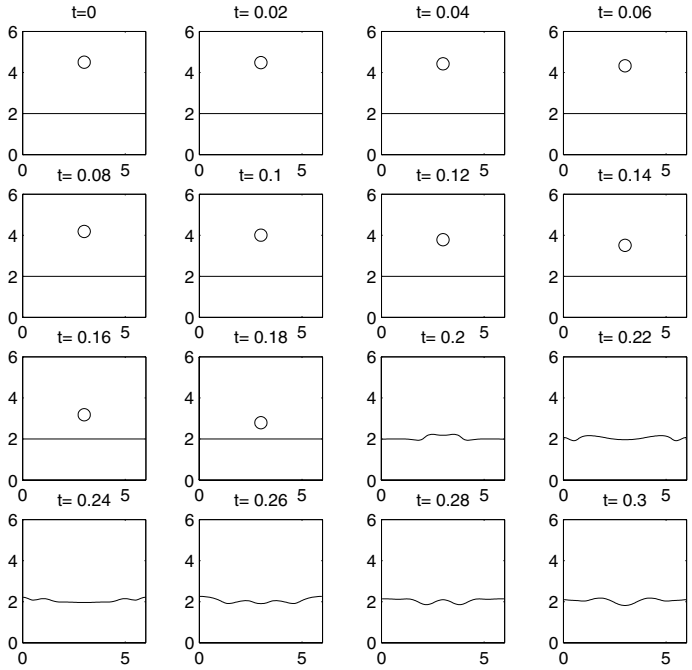

Fig. 16. Falling droplet from $t = 0$ to $t = 3.5$, 0.5 contour of Φ.

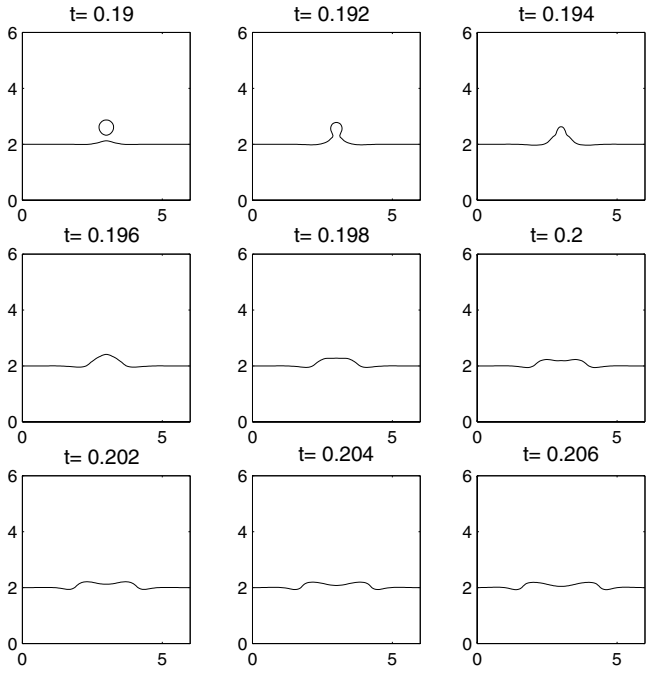

Fig. 17. Falling droplet, close to surface.

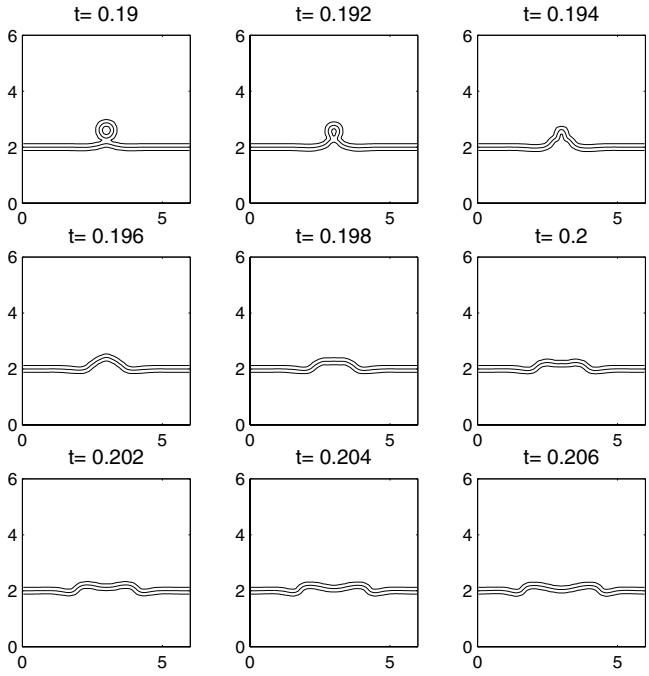

Fig. 18. Falling droplet, close to surface. 0.05, 0.5 and 0.95 contours of Φ.

5.4. Falling droplet

Finally, a problem involving topological changes of the interface was studied: a small droplet of water falls through air until it hits a water surface. The initial state is shown in Fig. 15.

As in the previous section, we set $\rho_{\text{ref}} = 1.0 \times 10^3$ kg/m^3, $\mu_{\text{ref}} = 1.0 \times 10^{-3}$ N s/m^2, $\rho_1 = 1$, $\rho_2 = 0.0013$, $\mu_1 = 1$, and $\mu_2 = 0.016$ and $\sigma = 7.3 \times 10^{-2}$ N/m. By choosing $l_{\text{ref}} = 1.0 \times 10^{-3}$ m and $u_{\text{ref}} = 1.0 \times 10^{-2}$ m/s, we get $Re = 10$, $Fr = 0.10$ and $We = 0.0014$. The discretization parameters were chosen as $\Delta x = 0.06$, Δt by stability as in (17).

Results from a droplet falling is shown in Figs. 16 and 17. We see that in the air the droplet remains quite circular. This is expected since on this small length scale surface tension is large. The horizontal surface stays straight as the droplet is approaching. One might expect that the air under the droplet would create a small bump on the horizontal surface. However, on this small length scale these effects are too small to be apparent in the results. We also note that as the distance of the bubble and the surface becomes close to the thickness of the interface, the droplet slightly attracts the surface. This is a numerical effect due to the diffuse representation of interfaces. As the droplet hits the water, waves propagating towards the wall are generated. Finally the waves are damped. We see that our method has no problem dealing with the topological change of the interface. In Fig. 18, the three contour lines corresponding to $\Phi = 0.05$, $\Phi = 0.5$ and $\Phi = 0.95$ are shown. We note that the interface keeps it thickness even as the droplet hits the surface.

6. Conclusions

We have constructed a numerical method for the advection of an interface in a divergence free velocity field. The method is conservative and the thickness of the diffuse interface is kept constant. Our method is easy to implement and the extension to three dimensions is straight forward. No special care has to be taken concerning topology changes, since this is automatically incorporated in the method. We have used second order approximations and numerical tests have also shown an actual order of accuracy of about two. Mass conservation is significantly better compared to the standard level set method.

Since our method is based on a certain smooth level set function together with a set of differential equations, other numerical methods can easily be applied. For example, higher order accurate and/or finite element discretization could be used. In this way, it should be possible to construct a conservative method with order greater than two.

Acknowledgments

The authors thank Gustav Amberg, Department of Mechanics, KTH, for helpful discussions on fluid dynamics. This work was supported by SSF Grant A3 02:123.

Appendix A. TVD method for advection

The TVD method for the advection of Φ using the upwind scheme together with a piecewise linear reconstruction can be summarized as follows.

A piecewise linear reconstruction of Φ is made. On each cell we have

$$\Phi(x, y) = \Phi_{i,j} + s^x_{i,j}(x - x_{i,j}) + s^y_{i,j}(y - y_{i,j}).$$

The slopes $s^x_{i,j}$ and $s^y_{i,j}$ are calculated by:

$$s^x_{i,j} = \mathrm{Lim}\left(\frac{\Phi_{i+1,j}-\Phi_{i,j}}{\Delta x}, \frac{\Phi_{i,j}-\Phi_{i-1,j}}{\Delta x}\right), \tag{A.1}$$

$$s^y_{i,j} = \mathrm{Lim}\left(\frac{\Phi_{i,j+1}-\Phi_{i,j}}{\Delta y}, \frac{\Phi_{i,j}-\Phi_{i,j-1}}{\Delta y}\right), \tag{A.2}$$

where $\mathrm{Lim}(x,y)$ defines the limiter. The Superbee limiter is defined as

$$\mathrm{Lim}(x,y) = \begin{cases} \mathrm{sign}(x)\max(|x|,|y|) & \text{if } |x|/2 \leqslant |y| \leqslant 2|x| \quad \text{and} \quad xy > 0, \\ 2\mathrm{sign}(x)\min(|x|,|y|) & \text{if } |x|/2 \geqslant |y| \quad \text{or} \quad |y| \geqslant 2|x| \quad \text{and} \quad xy > 0, \\ 0 & \text{if } xy < 0. \end{cases}$$

For the definition of other limiter, e.g. the minmod limiter, see for example [11].

The evolution of $\Phi_{i,j}$ is given by

$$\frac{\mathrm{d}\Phi_{i,j}}{\mathrm{d}t} = -\frac{1}{\Delta x}(F_{i+\frac{1}{2},j} - F_{i-\frac{1}{2},j}) - \frac{1}{\Delta y}(G_{i,j+\frac{1}{2}} - G_{i,j-\frac{1}{2}}), \tag{A.3}$$

where the fluxes are approximated using the upwind scheme for the linear reconstruction defined by the Superbee limiter:

$$F_{i+\frac{1}{2},j} = \max(u_{i+\frac{1}{2},j},0)\Phi^-_{i+\frac{1}{2},j} + \min(u_{i+\frac{1}{2},j},0)\Phi^+_{i+\frac{1}{2},j},$$
$$G_{i,j+\frac{1}{2}} = \max(v_{i,j+\frac{1}{2}},0)\Phi^-_{i,j+\frac{1}{2}} + \min(v_{i,j+\frac{1}{2}},0)\Phi^+_{i,j+\frac{1}{2}}.$$

Here

$$\Phi^-_{i+\frac{1}{2},j} = \Phi_{i,j} + \frac{\Delta x}{2}s^x_{i,j}, \quad \Phi^-_{i,j+\frac{1}{2}} = \Phi_{i,j} + \frac{\Delta y}{2}s^y_{i,j},$$
$$\Phi^+_{i+\frac{1}{2},j} = \Phi_{i+1,j} - \frac{\Delta x}{2}s^x_{i+1,j}, \quad \Phi^+_{i,j+\frac{1}{2}} = \Phi_{i,j+1} - \frac{\Delta y}{2}s^y_{i,j+1}.$$

Finally, we discretize in time using an explicit second order TVD Runge–Kutta. We rewrite the system of ODE:s in (A.3) as

$$\frac{\mathrm{d}\vec{\Phi}}{\mathrm{d}t} = \mathscr{F}(\vec{\Phi}).$$

$\vec{\Phi}$ is a vector containing all of the grid values $\Phi_{i,j}$. The second order Runge–Kutta we used is defined by:

$$\vec{\Phi}^* = \vec{\Phi}^n + \Delta t\mathscr{F}(\vec{\Phi}^n),$$
$$\vec{\Phi}^{**} = \vec{\Phi}^* + \Delta t\mathscr{F}(\vec{\Phi}^*),$$
$$\vec{\Phi}^{n+1} = \tfrac{1}{2}(\vec{\Phi}^n + \vec{\Phi}^{**}).$$

Appendix B. Discretization of the Navier–Stokes equations

The incompressible Navier–Stokes equations we are solving are given by:

$$\nabla\cdot\vec{u} = 0,$$

$$\vec{u}_\mathrm{t} + (\vec{u}\cdot\nabla)\vec{u} = -\frac{\nabla p}{\rho} + \frac{1}{\rho Re}\nabla\cdot\left(\mu\left(\nabla\vec{u} + (\nabla\vec{u})^\mathrm{T}\right)\right) + \frac{1}{Fr^2}\vec{e}_\mathrm{g} + \frac{1}{\rho We}\widetilde{F}_\mathrm{sv}.$$

We discretize using an extended version of the method described in [14]:

$$u^{n+1}_{i+\frac{1}{2},j} = u^n_{i+\frac{1}{2},j} + Q^n_{i+\frac{1}{2},j} - \frac{\Delta t}{\Delta x}\frac{p^{n+1}_{i+1,j} - p^{n+1}_{i,j}}{\rho^n_{i+\frac{1}{2},j}},$$

$$v^{n+1}_{i,j+\frac{1}{2}} = v^n_{i,j+\frac{1}{2}} + R^n_{i,j+\frac{1}{2}} - \frac{\Delta t}{\Delta y}\frac{p^{n+1}_{i,j+1} - p^{n+1}_{i,j}}{\rho^n_{i,j+\frac{1}{2}}}$$

with:

$$Q^n_{i+\frac{1}{2},j} = \Delta t\left(-uu_x - vu_y + \frac{(2\mu u_x)_x + (\mu(u_y + v_x))_y}{\rho Re} + \frac{1}{\rho We}F^x_{\mathrm{sv}}\right)^n_{i+\frac{1}{2},j},$$

$$R^n_{i,j+\frac{1}{2}} = \Delta t\left(-uv_x - vv_y + \frac{(2\mu v_y)_y + (\mu(u_y + v_x))_x}{\rho Re} + \frac{1}{Fr^2} + \frac{1}{\rho We}F^y_{\mathrm{sv}}\right)^n_{i,j+\frac{1}{2}}.$$

The discretization of the surface tension is done in the following way. The divergence of $\hat{n}$ is first approximated as

$$\left(\nabla\cdot\frac{\nabla\Phi}{|\nabla\Phi|}\right)_{i,j} = \frac{1}{2\Delta x}\left(\frac{(\Phi_x)_{i+1,j}}{|(\nabla\Phi)_{i+1,j}|} - \frac{(\Phi_x)_{i-1,j}}{|(\nabla\Phi)_{i-1,j}|}\right) + \frac{1}{2\Delta y}\left(\frac{(\Phi_y)_{i,j+1}}{|(\nabla\Phi)_{i,j+1}|} - \frac{(\Phi_y)_{i,j-1}}{|(\nabla\Phi)_{i,j-1}|}\right),$$

where the gradient of Φ is calculated using

$$(\nabla\Phi)_{i,j} = (\Phi_x)_{i,j}\hat{x} + (\Phi_y)_{i,j}\hat{y} = \frac{\Phi_{i+1,j} - \Phi_{i-1,j}}{2\Delta x}\hat{x} + \frac{\Phi_{i,j+1} - \Phi_{i,j-1}}{2\Delta y}\hat{y}$$

and

$$|(\nabla\Phi)_{i,j}| = \sqrt{(\Phi_x)^2_{i,j} + (\Phi_y)^2_{i,j}}.$$

Finally, we can calculate the surface tension:

$$(F^x_{\mathrm{sv}})_{i+\frac{1}{2},j} = \frac{1}{2}\left(\left(\nabla\cdot\frac{\nabla\Phi}{|\nabla\Phi|}\right)_{i,j}(\Phi_x)_{i,j} + \left(\nabla\cdot\frac{\nabla\Phi}{|\nabla\Phi|}\right)_{i+1,j}(\Phi_x)_{i+1,j}\right),$$

$$(F^y_{\mathrm{sv}})_{i,j+\frac{1}{2}} = \frac{1}{2}\left(\left(\nabla\cdot\frac{\nabla\Phi}{|\nabla\Phi|}\right)_{i,j}(\Phi_y)_{i,j} + \left(\nabla\cdot\frac{\nabla\Phi}{|\nabla\Phi|}\right)_{i,j+1}(\Phi_y)_{i,j+1}\right).$$

The other terms of $Q^n_{i+\frac{1}{2},j}$ are discretized by:

$$(uu_x)_{i+\frac{1}{2},j} = u_{i+\frac{1}{2},j}\cdot\frac{u_{i+\frac{3}{2},j} - u_{i-\frac{1}{2},j}}{2\Delta x},$$

$$(vu_y)_{i+\frac{1}{2},j} = \frac{1}{4}(v_{i,j+\frac{1}{2}} + v_{i,j-\frac{1}{2}} + v_{i+1,j+\frac{1}{2}} + v_{i+1,j-\frac{1}{2}})\cdot\frac{u_{i+\frac{1}{2},j+1} - u_{i+\frac{1}{2},j-1}}{2\Delta y},$$

$$\left((\mu u_x)_x\right)_{i+\frac{1}{2},j} = \frac{\mu_{i+1,j}\left(u_{i+\frac{3}{2},j} - u_{i+\frac{1}{2},j}\right) - \mu_{i,j}\left(u_{i+\frac{1}{2},j} - u_{i-\frac{1}{2},j}\right)}{(\Delta x)^2},$$

$$\left((\mu u_y)_y\right)_{i+\frac{1}{2},j} = \frac{\mu_{i+\frac{1}{2},j+\frac{1}{2}}(u_{i+\frac{1}{2},j+1} - u_{i+\frac{1}{2},j}) - \mu_{i+\frac{1}{2},j-\frac{1}{2}}(u_{i+\frac{1}{2},j} - u_{i+\frac{1}{2},j-1})}{(\Delta y)^2},$$

$$\left((\mu v_x)_y\right)_{i+\frac{1}{2},j} = \frac{\mu_{i+\frac{1}{2},j+\frac{1}{2}}(v_{i+1,j+\frac{1}{2}} - v_{i,j+\frac{1}{2}}) - \mu_{i+\frac{1}{2},j-\frac{1}{2}}(v_{i+1,j-\frac{1}{2}} - v_{i,j-\frac{1}{2}})}{\Delta x\Delta y}.$$

To calculate ρ and μ at cell faces we use:

$$(\rho)_{i,j} = \rho_1 + (\rho_2 - \rho_1)\cdot \Phi_{i,j},$$
$$(\rho)_{i,j+\frac{1}{2}} = \tfrac{1}{2}((\rho)_{i,j} + (\rho)_{i,j+1}),$$
$$(\rho)_{i+\frac{1}{2},j} = \tfrac{1}{2}((\rho)_{i,j} + (\rho)_{i+1,j})$$

and, respectively, for μ.

We require $\vec{u}$ to be divergence free at t^{n+1}, i.e., $(\nabla\cdot\vec{u})_{i,j}^{n+1} = 0$, where

$$(\nabla\cdot\vec{u})_{i,j}^{n+1} = \frac{u_{i+\frac{1}{2},j} - u_{i-\frac{1}{2},j}}{\Delta x} + \frac{v_{i,j+\frac{1}{2}} - v_{i,j-\frac{1}{2}}}{\Delta y}.$$

This yields the pressure implicitly as

$$\left(\nabla\cdot\left(\frac{\nabla p^{n+1}}{\rho^n}\right)\right)_{i,j} = (Q_x + R_y)_{i,j}^n,$$

which is discretized as

$$\frac{1}{(\Delta x)^2}\left(\frac{p_{i+1,j}^{n+1} - p_{i,j}^{n+1}}{\rho_{i+\frac{1}{2},j}^n} - \frac{p_{i,j}^{n+1} - p_{i-1,j}^{n+1}}{\rho_{i-\frac{1}{2},j}^n}\right) + \frac{1}{(\Delta y)^2}\left(\frac{p_{i,j+1}^{n+1} - p_{i,j}^{n+1}}{\rho_{i,j+\frac{1}{2}}^n} - \frac{p_{i,j}^{n+1} - p_{i,j-1}^{n+1}}{\rho_{i,j-\frac{1}{2}}^n}\right)$$
$$= \left(\frac{Q_{i+\frac{1}{2},j}^n - Q_{i-\frac{1}{2},j}^n}{\Delta x} + \frac{R_{i,j+\frac{1}{2}}^n - R_{i,j-\frac{1}{2}}^n}{\Delta y}\right).$$

This linear system was solved using a direct solver for banded matrices. Alternatively some iterative method such as a preconditioned conjugate gradient method or a multigrid method could have been used.

References

[1] W. Noh, P. Woodward, SLIC (simple line interface calculation), in: A. van de Vooren, P. Zandbergen (Eds.), Proceedings of the 5th International Conference on Fluid Dynamics, vol. 59 of Lecture Notes in Physics, 1976, pp. 330–340.
[2] R. Scardovelli, S. Zaleski, Direct numerical simulation of free-surface and interfacial flow, Ann. Rev. Fluid Mech. 31 (1999) 567–603.
[3] S. Unverdi, G. Tryggvason, A front-tracking method for viscous, incompressible, multi-fluid flows, J. Comput. Phys. 100 (1992) 25–37.
[4] S. Osher, R. Fedkiw, Level Set Methods and Dynamic Implicit Surfaces, Springer-Verlag, Berlin, 2003.
[5] J. Sethian, Level Set Methods and Fast Marching Methods, Cambridge University Press, Cambridge, 1999.
[6] M. Sussman, P. Smereka, S. Osher, A level set approach for computing solutions to incompressible two-phase flow, J. Comput. Phys. 114 (1994) 146–159.
[7] M. Sussman, E. Fatemi, P. Smereka, S. Osher, An improved level set method for incompressible two-phase flows, Comp. Fluid 27 (1998) 663–680.
[8] A.-K. Tornberg, B. Enhquist, A finite element based level set method for multiphase flow applications, Comput. Visual. Sci. 3 (2000) 93–101.
[9] M. Sussman, E. Puckett, A coupled level set and volume-of-fluid method for computing 3d and axisymmetric incompressible two-phase flows, J. Comput. Phys. 162 (2000) 301–337.
[10] D. Enright, R. Fedkiw, J. Ferziger, I. Mitchell, A hybrid particle level set method for improved interface capturing, J. Comput. Phys. 183 (2002) 83–116.
[11] R. Leveque, Finite Volume Methods for Hyperbolic Problems, Cambridge University Press, Cambridge, 2002.
[12] A. Harten, The artificial compression method for computation of shocks and contact discontinuities. I. Single conservation laws, Comm. Pure Appl. Math. (1977) 611–638.
[13] J.U. Brackbill, D. Kothe, C. Zemach, A continuum method for modeling surface tension, J. Comput. Phys. 100 (1992) 335–353.
[14] F. Harlow, E. Welch, Numerical calculation of time-dependent viscous incompressible flow of fluids with free surface, Phys. Fluids 8 (1965) 2182.